Acta Crystallographica Section A
Foundations of Crystallography
ISSN 0108-7673

Received 28 November 2011
Accepted 6 March 2012

Temperature diffuse scattering of nanocrystals

K. R. Beyerlein,[a,b]* M. Leoni[b] and P. Scardi[b]

[a]Materials Science and Engineering Department, Georgia Institute of Technology, Atlanta, GA, USA, and [b]Department of Materials Engineering and Industrial Technology, University of Trento, Trento, Italy. Correspondence e-mail: kbeyerlein3@gatech.edu

The effects of thermal vibrations on X-ray powder diffraction patterns are discussed. Special considerations for extremely small crystallites are described, including the occurrence of surface and edge vibrational modes, and a restriction on the maximum phonon wavelength. In doing so, a complete temperature diffuse scattering (TDS) model is presented, which includes the influence of these features on: the Debye–Waller parameter; first-order TDS; and higher-order TDS terms. The importance of using an accurate TDS representation is studied as a function of temperature and crystallite size. It is found that a misrepresentation of the TDS for small crystallites can lead to an error in the determined Debye–Waller parameter on the order of 20–40% and a slight overestimation of the peak broadening. While the presented theory is primarily developed considering X-ray scattering, the same expressions are expected to describe the TDS in faster-than-sound neutron powder diffraction measurements.

1. Introduction

The thermal motion of atoms in a crystal displaces them from their ideal lattice configuration, which in turn diminishes the scattered intensity in the Bragg spots. This attenuation can be expressed as

$$I = \exp(-2M)I_{\rm Bragg} + I_{\rm TBG}, \qquad (1)$$

where the Bragg component, $I_{\rm Bragg}$, of the observed intensity, I, is scaled by the Debye–Waller factor, $\exp(-2M)$. The intensity from a Bragg spot is not lost, but is spread diffusely in reciprocal space, making up what we will call the thermal background intensity, $I_{\rm TBG}$. If one assumes that atomic motion is completely random, and uncorrelated, Debye has shown that the thermal diffuse background is given by a smooth analytical function, independent of the crystal structure (Debye, 1914). However, real thermal motion in a crystal lattice is manifested as vibrational waves, or phonons, which are ideal examples of *correlated* atomic motion. It has been well established that this correlated atomic motion results in what is known as temperature (or thermal) diffuse scattering (TDS) (Born & Huang, 1998; James, 1962). The TDS is commonly expanded as a series of terms composing the $I_{\rm TBG}$, with the lth order associated with scattering from l phonon modes. The scattered intensity from a crystallite containing phonons can then be written as

$$I = \exp(-2M)I_{\rm Bragg} + I_{\rm TDS_1} + I_{\rm TDS_2} + \ldots, \qquad (2)$$

where $I_{\rm TDS_1}$ represents the intensity due to the first-order TDS, $I_{\rm TDS_2}$ is the second-order TDS, and so on. In contrast to the smooth background found from random motion, the TDS can be highly directionally dependent and has peaks under the Bragg peaks.

Despite this knowledge, when analyzing an X-ray powder diffraction pattern, it is commonly assumed that the effect of the TDS is small and largely accounted for by fitting a smooth background. The many works of Suortti, Honkimäki and co-workers (Honkimäki & Suortti, 1992; Suortti, 1967, 1993) are exceptions, as they have described different ways of modeling the TDS background to improve Rietveld and line profile analysis of a number of systems.

The justification for ignoring the TDS in the case of large crystallites might be that the percentage of the intensity which is attributed to the TDS becomes small relative to the Bragg scattering. This can be reasoned by considering that the Bragg peak height scales as N^2, while the TDS peak is only linearly proportional to the number of atoms, N. However, by the same consideration, as the crystallite becomes smaller, the TDS can be expected to compose an observable fraction of the intensity and becomes an important consideration.

Therefore, it is the purpose of this study to investigate the case when the domain size becomes small, to determine the extent to which the TDS might influence the observed intensity profiles. In doing so, one must be cognizant of the fact that the vibrational characteristics of a small crystallite are different from those of a large crystallite. Therefore, a key aspect of the following work is to develop new models for the Debye–Waller factor and TDS which are appropriate for small crystallites. A series of simulated diffraction patterns will then be modeled using modern line profile analysis methods, intentionally approximating the TDS with a smooth function. The corresponding magnitudes of error in the obtained

domain size and Debye–Waller parameter are then studied as a function of temperature and crystal size.

2. Models for the temperature background

2.1. Empirical model: Chebyshev background

A common empirical approach to modeling the diffraction pattern background is to assume a series of Chebyshev polynomials of the first kind, $T_i(x)$, as in

$$I_{\rm TBG}(x) = \sum_{i=0}^{i_{\max}} a_i T_i(x), \quad (3)$$

and refine the scaling coefficients, a_i, to obtain the best fit. In this expression, x represents the abscissa of a diffraction pattern, which can be in terms of the scattering angle, 2θ, or the scattering vector magnitude, $s = 2\sin\theta/\lambda$, where λ is the wavelength of incident radiation. The Chebyshev polynomials are commonly defined in terms of a recursion relation following: $T_0(x) = 1$; $T_1(x) = x$; and $T_{n+1}(x) = 2xT_n(x) - T_{n-1}(x)$. They have the desired property that they are slowly varying, bounded and orthogonal in the interval $x \in [-1, 1]$. Therefore, one should map this interval to the abscissa of a diffraction pattern when evaluating the Chebyshev background (Press *et al.*, 2007). This decreases the correlation between the a_i coefficients and theoretically allows for the expansion of any function in terms of a series of Chebyshev polynomials. However, to avoid correlation with other parameters when fitting the diffraction pattern, it is best to keep the number of free parameters as low as possible. So, it is common to assume a series with somewhere between four and six orders of Chebyshev polynomials.

2.2. Debye model: the effect of random atomic motion

The expected background from purely random thermal motion can be derived following the assumptions of the Debye model for the specific heats of solids (Debye, 1914). Then, the Debye temperature background for a system containing N identical atoms is shown to be

$$I_{\rm TBG}(s) = k(s)|f(s)|^2 N[1 - \exp(-2M)], \quad (4)$$

which gives the absolute value of the intensity in electron units (Warren, 1990). Here, the function $k(s)$ depends on the measurement geometry, and includes the effects of polarization and absorption, while $|f(s)|^2$ is the atomic scattering factor. Also, this expression shows that the same Debye–Waller factor, $\exp(-2M)$, which attenuates the Bragg intensity also governs the shape of the Debye TBG. Again, this form of the TBG comes directly from the assumption of uncorrelated thermal motion, and will be shown to only approximately account for the general trend of the TDS.

2.3. TDS model for small, cubic crystallites

A few different models to describe the TDS in a powder diffraction pattern from a cubic material have been developed by a number of authors in the literature (*e.g.* Suortti, 1967; Walker & Chipman, 1972; Warren, 1990; Willis & Pryor, 1975, and references therein). Generally, they differ only slightly in how the necessary integrals are treated and approximated. However, the literature contains a vast array of different notations concerning the TDS, and it should be noted that the following equations largely adhere to that found in the works of James (1962) and Warren (1990). In most cases, the lth-order term of the powder TDS, $I_{{\rm PTDS}_l}(s)$, can be cast in the form

$$I_{{\rm PTDS}_l}(s) = k(s)|f(s)|^2 N \exp(-2M)\frac{(2M)^l}{l!}\sum_{h,k,l} Q_l(s, s_{hkl}). \quad (5)$$

Here the function $Q_l(s, s_{hkl})$ is the normalized TDS peak, which contains the hkl-dependent shape of the lth-order TDS, and is positioned at the Bragg scattering vector, s_{hkl} (Warren, 1990). It is found directly from equation (5) to be defined as

$$Q_l(s, s_{hkl}) = \frac{I_{{\rm PTDS}_l}(s, s_{hkl})}{k(s)N|f(s)|^2\exp(-2M)(2M)^l/l!}. \quad (6)$$

We will utilize the approach of defining $Q_l(s, s_{hkl})$ and $2M$ functions in terms of the vibrational characteristics of the crystal, and derive appropriate expressions for the case of small crystallites.

2.3.1. Vibrational density of states. The vibrational density of states (VDOS) embodies the normal modes of vibration which are allowed in a crystallite. The VDOS for a small crystallite is expected to be different to that of a large, or infinite, crystal for a few reasons.

First, normal modes with wavelengths larger than twice the crystallite size cannot exist. An analogy of this exists in acoustics as the first harmonic of a rod with free boundary conditions is proportional to twice its length. This idea simply translates into atomic vibrations by defining a maximum allowable wavelength for the normal modes, $\lambda_{\max}$, which is inversely related to a lower limit of the allowed wavevector magnitudes, $g_{\min}$:

$$g_{\min} = 1/\lambda_{\max} \propto 1/2L, \quad (7)$$

where L is a measure of the crystallite size (Marshall & Wilenzick, 1966; Thiel, 1967). Strictly speaking, the shape of a crystallite can lead to a set of values for $g_{\min}$, corresponding to the size and symmetry of the crystal in each direction. However, in most cases, the specific shape dependence of this parameter is likely to have a small effect on the resulting TDS. Therefore, as a first-order approximation, we assume a spherically symmetric shape and define only one such $g_{\min}$ for a given crystallite. This assumption begins to break down for the case of crystallites with large aspect ratios, as in thin platelets or nanorods. However, in these cases we expect that our definition will be associated with a spatially averaged $g_{\min}$. This definition in terms of a single average value also becomes important later, as it simplifies the evaluation of the powder integral in equation (25).

A second difference in the VDOS of a small, isolated crystallite is that it becomes increasingly influenced by surface and edge vibrational modes. The dimensionality of the influence from these kinds of modes on the VDOS is found in the

expressions derived by Maa (1939), and Bolt (1939), considering acoustic vibrations in a rectangular room with 'clamped' walls. Under the long-wavelength approximation, we assume a simple, linear dispersion relationship, $\nu_g = c_s g$; where ν_g is the vibration frequency associated with the wavevector g, and the average speed of sound, c_s, is given by that of an elastically isotropic material as

$$\frac{1}{c_s^2} = \frac{1}{3}\left(\frac{1}{c_l^2} + \frac{2}{c_t^2}\right), \tag{8}$$

with c_l and c_t being the longitudinal and transverse speeds of sound, respectively (Walker & Chipman, 1972; Warren, 1990). Then one finds that the Maa VDOS for a wavevector, $\mathbf{g}$, becomes

$$\rho(\mathbf{g}) = V\alpha_3 + \frac{S\alpha_2}{8}\frac{1}{g} + \frac{E\alpha_1}{32\pi}\frac{1}{g^2}. \tag{9}$$

Here V, S and E are the volume, surface area and edge length of the crystallite, respectively. Also, the α_i constants, found from averaging the longitudinal and transverse polarizations, are

$$\alpha_i = \frac{1 + 2(c_l/c_t)^i}{\left\{[1 + 2(c_l/c_t)^2]/3\right\}^{i/2}}. \tag{10}$$

By integrating $\rho(\mathbf{g})$ over all orientations of the vector $\mathbf{g}$, one finds the more commonly referenced total density of states, $\Gamma(g)$. Then, from equation (9), this density is

$$\Gamma(g) = 4\pi g^2 \rho(\mathbf{g}) = 4\pi\left(V\alpha_3 g^2 + \frac{S\alpha_2}{8}g + \frac{E\alpha_1}{32\pi}\right). \tag{11}$$

Beyond Maa's work with parallelepipeds, this general expression was later found to also hold for the cases of volumes exhibiting spherical and cylindrical symmetry (Roe, 1941), and is believed to be true for most shapes. The shape dependence is then embodied in the expressions for the volume, surface area and total edge length – examples of which will be given later.

The integral of the density of states must equal the number of independent modes in the crystallite, which is approximately $3N$. Given the Maa VDOS, Montroll (1950) has used this criterion to solve for an outer limit, g_{max}, but in doing so assumes $g_{min} = 0$. This solution for g_{max} can be adapted to our case, where $g_{min} > 0$, by defining a new effective total number of modes as

$$3N' = 3N + \frac{4\pi g_{min}^3}{3}V\alpha_3 + \frac{\pi g_{min}^2}{4}S\alpha_2 + \frac{g_{min}}{8}E\alpha_1. \tag{12}$$

Then, the expression for g_{max} which correctly normalizes the VDOS is given by

$$g_{max} = \gamma_1\left(\frac{3N'}{4\pi V}\right)^{1/3}\left[1 - \frac{\gamma_2\pi S}{12N'}\left(\frac{3N'}{4\pi V}\right)^{2/3} + O(N'^{-2/3})\right], \tag{13}$$

with

$$\gamma_i = \frac{\left\{[1 + 2(c_l/c_t)^2]/3\right\}^{i/2}}{\left\{[1 + 2(c_l/c_t)^3]/3\right\}^{i/3}}. \tag{14}$$

2.3.2. The Debye–Waller factor. The exponent of the Debye–Waller (D–W) factor, $2M$, can be found from evaluating

$$2M = \frac{s^2 h}{2Nm}\sum_{g,j}\frac{\coth(h\nu_{gj}/2k_B T)\cos^2(\theta_{\mathbf{s},\mathbf{e}_{g,j}})}{\nu_{gj}}, \tag{15}$$

where m is the atomic mass and h is the Planck constant (James, 1962). The summation is intended to be over all possible wavevectors, g, and vibration polarizations, $j \in \{1, 2, 3\}$. The variables ν_{gj} and $\theta_{\mathbf{s},\mathbf{e}_{gj}}$ are then, respectively, the vibration frequency, and the angle between the scattering vector, $\mathbf{s}$, and a unit vector describing the vibration direction, $\mathbf{e}_{gj}$. At high enough temperatures, the energy distribution function can be approximated as: $\coth(h\nu_{gj}/2k_B T) \cong 2k_B T/h\nu_{gj}$, with k_B signifying the Boltzmann constant and T denoting the temperature. Then, assuming the average speed of sound defined by equation (8), and a linear dispersion relationship as before, the D–W exponent reduces to

$$2M = \frac{s^2 k_B T}{Nmc_s^2}\sum_g \frac{1}{g^2}. \tag{16}$$

The summation over g can be expressed as an integral over the density of states, as in

$$2M = \frac{s^2 k_B T}{Nmc_s^2}\int_{g_{min}}^{g_{max}}\frac{\rho(g)}{g^2}4\pi g^2\,\mathrm{d}g. \tag{17}$$

Now, assuming the density of states defined in equation (9), the D–W exponent is found to be

$$2M = A(s)\left[4\pi\alpha_3(g_{max} - g_{min}) + \frac{\pi S\alpha_2}{2V}\ln\left(\frac{g_{max}}{g_{min}}\right) + \frac{E\alpha_1}{8V}\left(g_{min}^{-1} - g_{max}^{-1}\right)\right], \tag{18a}$$

$$= A(s)\left[(Y_0)_V + (Y_0)_S + (Y_0)_E\right], \tag{18b}$$

where

$$A(s) = \frac{s^2 k_B T V}{Nmc_s^2}, \tag{19}$$

and the variables $(Y_0)_V$, $(Y_0)_S$ and $(Y_0)_E$, are used to denote the corresponding functions in equation (18*a*), which, respectively, account for the volume, surface and edge contributions to the D–W exponent. When evaluating this expression for a mono-atomic lattice, it is possible to make the approximation $V/N = v_a$, where v_a is the atomic volume.

This D–W exponent is related to the D–W parameter, B_{iso}, by $2M = B_{iso}s^2/2$, where the 'iso' subscript signifies the assumption of isotropic thermal motion, which was implicit in

our calculation of $2M$. Therefore, the D–W parameter is given as

$$B_{\rm iso} = \frac{2k_{\rm B}TV}{Nmc_{\rm s}^2}\left[(Y_0)_{\rm V} + (Y_0)_{\rm S} + (Y_0)_{\rm E}\right]. \qquad (20)$$

Schoening has also assumed the same form of the VDOS and arrived at a similar expression for $B_{\rm iso}$ (Schoening, 1968), but only explicitly solves for this parameter for the case where the shape of the crystallite is a cube. Furthermore, he makes an assumption that $g_{\rm min} = 0$ when evaluating $g_{\rm max}$. In contrast, equation (20) is correctly normalized and expressed generally for any shape.

As previously mentioned, the specific shape dependence in our theory comes from the surface-area-to-volume and edge-length-to-volume ratios. For the case of a sphere it is straightforward to show that these functions can be parametrized in terms of the diameter, D, as $S/V = 6/D$ and $E/V = 0$, while for the case of a cube these functions are $S/V = 6/L$ and $E/V = 12/L^2$, where L is the side length of a cube.

The contribution from the surface and edge modes then makes $B_{\rm iso}$ a function of the crystallite size. This theoretical dependence is illustrated in Fig. 1(*a*), for the case of Al crystallites,[1] assuming a spherical shape. It is seen that the resulting $B_{\rm iso}$ increases with decreasing sphere diameter and approaches an asymptotic value with larger size. The nearly linear trend of $B_{\rm iso}$ *versus* $1/D$ shown in Fig. 1(*a*) is expected because of its dependence on the S/V ratio. Meanwhile, the slight deviation from linearity comes from the size dependence of $g_{\rm min}$ and $g_{\rm max}$, which enter into the Y_0 functions. The predictions of the model are consistent with previous works, as an increasing $1/D$ dependence of the thermal component on the D–W factor has also been reported by numerous studies in the literature (Eastman & Fitzsimmons, 1995; Inagaki *et al.*, 1983; Zhao & Lu, 1997). This trend is analogous to an effective lowering of the Debye temperature, $\Theta_{\rm D}$, or an increased mean-squared displacement of atoms due to thermal vibrations, $\langle u_d^2 \rangle$, which has also been reported in studies of the specific heat and melting of nanocrystallites (Balerna & Mobilio, 1986; Couchman & Karasz, 1977; Sadaiyandi, 2009; Solliard, 1984; Xiong *et al.*, 2011).

The dependence of the D–W parameter on the ratio of the longitudinal and transverse wave velocities is depicted in Fig. 1(*b*). Using the physical parameters which describe Al, the D–W factor is found to be highly sensitive to this ratio, varying from 0.5 to 2.5 Å^2. Also, by comparing the trends for the different crystal sizes, it is found that as the crystal gets smaller this dependence slightly increases. A rather broad range of possible velocity ratios is depicted here to illustrate the predicted limits of the D–W relation; however, most materials fall in the $c_{\rm l}/c_{\rm t}$ range from 0.5 to 1.5.

2.3.3. First-order TDS. Now, considering the contributions to the thermal background, the first-order TDS can be found from evaluating (James, 1962; Warren, 1990)

[1] In this and other examples, Al was chosen because it is nearly elastically isotropic, which is consistent with assumptions made in deriving the theory.

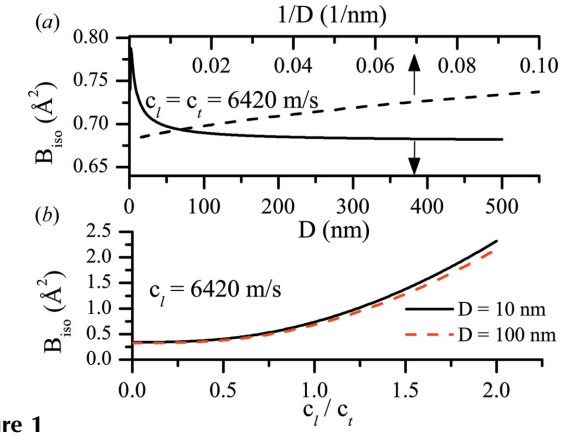

Figure 1
The dependences of the Debye–Waller parameter ($B_{\rm iso}$), as described by equation (20), (*a*) on the crystallite diameter and (*b*) on the ratio of the speed of sound are depicted. The physical constants used to simulate this quantity for the Al spheres at 300 K are: $a = 0.404$ nm; $V/N = 0.01648$ nm^3 per atom; and $m = 26.98$ atomic mass units.

$$I_{\rm TDS_1}(\mathbf{s}) = k(s)|f(s)|^2 \exp(-2M)\frac{s^2 h}{4Nmc_{\rm s}^2} \times \sum_{g,j}\left\{\frac{\coth(h\nu_{gj}/2k_{\rm B}T)\cos^2(\theta_{\mathbf{s},\mathbf{e}_{g,j}})}{\nu_{gj}} \times \sum_{m,n}\exp[-2\pi i(\mathbf{s}+\mathbf{g})\cdot\mathbf{d}_{mn}] + \exp[-2\pi i(\mathbf{s}-\mathbf{g})\cdot\mathbf{d}_{mn}]\right\}. \qquad (21)$$

The second summation evaluates all relative distance vectors between atoms, $\mathbf{d}_{mn}$. When $g = 0$, this summation becomes the interference function which gives rise to the Bragg spots. Now, by summing this expression over $\mathbf{g}$, the first-order TDS is then essentially a convolution of the ideal TDS effect with the Bragg intensity. For the purpose of theoretically evaluating the ideal TDS peak shape, we will treat the Bragg spots as series of delta functions weighted by the integrated Bragg intensity, then

$$\sum_{m,n}\exp[-2\pi i(\mathbf{s}\pm\mathbf{g})\cdot\mathbf{d}_{mn}] = \sum_{h,k,l} N\delta(\mathbf{s}-\mathbf{s}_{hkl}-\mathbf{g}). \qquad (22)$$

However, as will be discussed later, it must be kept in mind that the resulting form of the TDS should be convolved with the normalized Bragg intensity to depict the observable TDS effect (Suortti, 1967). Then, using the high-temperature approximation and the same average speed of sound as before, the first-order TDS is given by

$$I_{\rm TDS_1}(\mathbf{s}) = k(s)|f(s)|^2\exp(-2M)\frac{s^2 k_{\rm B}T}{mc_{\rm s}^2}\sum_{h,k,l}\int_{\mathbf{g}}\frac{\rho(g)}{g^2} \times \delta(\mathbf{s}-\mathbf{s}_{hkl}-\mathbf{g})\,{\rm d}v_{\mathbf{g}}. \qquad (23)$$

The delta function is only non-zero when $\mathbf{g} = \mathbf{s} - \mathbf{s}_{hkl}$, and the integral over $\mathbf{g}$ is taken over the first Brillouin zone, which can be expressed in terms of dimensionless parameters weighted by the Brillouin zone volume, $1/v_{\rm a}$. Again, using the density of states given by equation (9), the first-order TDS attributed to a given *hkl* is found to be

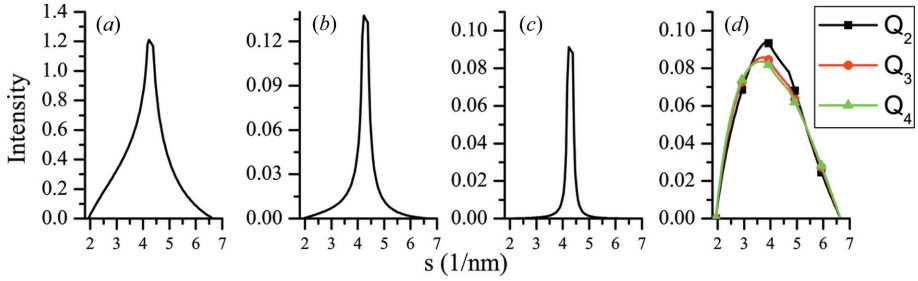

Figure 2
The contributions to Q_1 of the (*a*) volume, (*b*) surface and (*c*) edge vibration modes for the Al ($a = 0.404$ nm) 111 peak are compared. In evaluating equation (29), cubes with an edge length of 5 nm and $c_l/c_t = 1$ were assumed. (*d*) Also shown for this peak are the resulting forms of some of the higher-order functions, Q_l, given by equation (43).

$$I_{\mathrm{TDS}_1}(\mathbf{s},\mathbf{s}_{hkl}) = k(s)|f(s)|^2\exp(-2M)\frac{s^2Vk_\mathrm{B}T}{v_\mathrm{a}mc_\mathrm{s}^2} \times\left[\frac{\alpha_3}{|\mathbf{s}-\mathbf{s}_{hkl}|^2}+\frac{\alpha_2 S}{8V}\frac{1}{|\mathbf{s}-\mathbf{s}_{hkl}|^3}+\frac{\alpha_1 E}{32\pi V}\frac{1}{|\mathbf{s}-\mathbf{s}_{hkl}|^4}\right]. \tag{24}$$

The powder intensity is found from the single-crystal intensity by taking the powder average

$$I_\mathrm{P}(s) = \frac{1}{4\pi s^2}\int I(\mathbf{s})\,\mathrm{d}\Omega. \tag{25}$$

This integral of the intensity in equation (24) is readily evaluated to find the first-order powder TDS[2] as

$$I_{\mathrm{PTDS}_1}(s,s_{hkl}) = \frac{k(s)m_{hkl}|f(s)|^2\exp(-2M)}{4ss_{hkl}}\frac{s^2Vk_\mathrm{B}T}{v_\mathrm{a}mc_\mathrm{s}^2} \times\left[\alpha_3\ln\left(\frac{x_\mathrm{max}}{x_0}\right)+\frac{\alpha_2 S}{16V}\left(x_0^{-1/2}-x_\mathrm{max}^{-1/2}\right) +\frac{\alpha_1 E}{32\pi V}\left(x_0^{-1}-x_\mathrm{max}^{-1}\right)\right], \tag{26}$$

where m_{hkl} is the multiplicity of a peak,

$$x_0 = \begin{cases} s^2+s_{hkl}^2-2ss_{hkl} & (s-s_{hkl})\geq g_\mathrm{min} \\ g_\mathrm{min}^2 & (s-s_{hkl})<g_\mathrm{min}\end{cases}, \tag{27}$$

and

$$x_\mathrm{max} = g_\mathrm{max}^2. \tag{28}$$

Urban (1975) has also derived a similar expression for the first-order TDS from the Maa VDOS. However, in doing so he assumed a different form for the average speed of sound and did not express the full scale factor of the TDS in electron units, as presented here.

From equation (6), the normalized first-order powder TDS is given by

$$Q_1(s,s_{hkl}) = \frac{1}{v_\mathrm{a}}\frac{m_{hkl}}{4ss_{hkl}}\left[\alpha_3\ln\left(\frac{x_\mathrm{max}}{x_0}\right)+\frac{S\alpha_2}{8V}\frac{1}{2}\left(x_0^{-1/2}-x_\mathrm{max}^{-1/2}\right) +\frac{E\alpha_1}{32\pi V}\left(x_0^{-1}-x_\mathrm{max}^{-1}\right)\right]\Big/[(Y_0)_\mathrm{V}+(Y_0)_\mathrm{S}+(Y_0)_\mathrm{E}]. \tag{29}$$

[2] It is worth noting that the Lorentz factor for a powder pattern is already contained in the $1/ss_{hkl}$ term in equation (26).

Examples of the respective volume, surface and edge contributions to the normalized, first-order TDS of the Al 111 peak are shown in Fig. 2. The intensity scale of these peaks is that given directly from equation (29), and is, respectively, governed by the S/V and E/V ratios for a crystallite shape.

2.3.4. Higher-order TDS. Approximations for the higher-order TDS terms can be found following the approach of Warren (1990). The *l*th-order TDS intensity can be expressed as

$$I_{\mathrm{TDS}_l}(\mathbf{s}) = k(s)|f(s)|^2\exp(-2M)\sum_{m,n}\exp(2\pi i\mathbf{s}\cdot\mathbf{d}_{mn})\frac{Y_{mn}^l}{l!}. \tag{30}$$

Again, using the same set of assumptions as in the first-order case, the parameter Y_{mn} is given by

$$Y_{mn} = \frac{s^2k_\mathrm{B}T}{Nmc_\mathrm{s}^2}\int\frac{\rho(g)}{g^2}\cos(2\pi\mathbf{g}\cdot\mathbf{d}_{mn})g^2\sin\theta\,\mathrm{d}g\,\mathrm{d}\theta\,\mathrm{d}\varphi. \tag{31}$$

Since our density of states is only dependent on the magnitude of the wavevector, the expression becomes

$$Y_{mn} = 4\pi A(s)\int_{g_\mathrm{min}}^{g_\mathrm{max}}\mathrm{sinc}(2\pi g d_{mn})\left(\alpha_3+\frac{S\alpha_2}{8V}\frac{1}{g}+\frac{L\alpha_1}{32\pi V}\frac{1}{g^2}\right)\mathrm{d}g. \tag{32}$$

Evaluating this integral, the Y_{mn} parameter is again found to be expressible in terms of its volume, surface and edge components, as

$$Y_{mn} = A(s)\left[(Y_{mn})_\mathrm{V}+(Y_{mn})_\mathrm{S}+(Y_{mn})_\mathrm{E}\right], \tag{33}$$

where

$$(Y_{mn})_\mathrm{V} = \frac{4\pi\alpha_3}{2\pi d_{mn}}\left[\mathrm{Si}(2\pi g_\mathrm{max}d_{mn})-\mathrm{Si}(2\pi g_\mathrm{min}d_{mn})\right], \tag{34}$$

$$(Y_{mn})_\mathrm{S} = 4\pi\frac{\alpha_2 S}{8V}[\mathrm{Ci}(2\pi g_\mathrm{max}d_{mn})-\mathrm{sinc}(2\pi g_\mathrm{max}d_{mn}) -\mathrm{Ci}(2\pi g_\mathrm{min}d_{mn})+\mathrm{sinc}(2\pi g_\mathrm{min}d_{mn})], \tag{35}$$

$$(Y_{mn})_{\rm E} = 4\pi(2\pi d_{mn})\frac{\alpha_1 L}{64\pi V} \times \left[-\frac{\cos(2\pi g_{\max} d_{mn})}{2\pi g_{\max} d_{mn}} - \frac{\mathrm{sinc}(2\pi g_{\max} d_{mn})}{2\pi g_{\max} d_{mn}} - \mathrm{Si}(2\pi g_{\max} d_{mn}) + \frac{\cos(2\pi g_{\min} d_{mn})}{2\pi g_{\min} d_{mn}} + \frac{\mathrm{sinc}(2\pi g_{\min} d_{mn})}{2\pi g_{\min} d_{mn}} + \mathrm{Si}(2\pi g_{\min} d_{mn})\right], \quad (36)$$

and $A(s)$ is defined in equation (19). Here $\mathrm{Si}(x)$ and $\mathrm{Ci}(x)$ denote the sine integral and cosine integral functions, respectively. Using the expression of equation (33), the lth-order TDS becomes

$$I_{\mathrm{TDS}_l}(\mathbf{s}) = k(s)|f(s)|^2 \exp(-2M) A(s)^l \sum_{m,n} \exp(2\pi i \mathbf{s}\cdot\mathbf{d}_{mn}) \times \frac{\left[(Y_{mn})_{\rm V} + (Y_{mn})_{\rm S} + (Y_{mn})_{\rm E}\right]^l}{l!}. \quad (37)$$

To allow for an analytical solution to the powder TDS, Warren *approximates* the exponential component of equation (30) as the sum of orientationally symmetric Bragg spots:

$$\exp(2\pi i \mathbf{s}\cdot\mathbf{d}_{mn}) \sim \sum_{hkl} \frac{1}{4\pi} \int_{\Omega} \exp(2\pi i \mathbf{q}_{hkl}\cdot\mathbf{d}_{mn})\,\mathrm{d}\Omega = \sum_{hkl} \mathrm{sinc}(2\pi q_{hkl} d_{mn}), \quad (38)$$

where $\mathbf{q}_{hkl} = \mathbf{s} - \mathbf{s}_{hkl}$. Then, using equation (37), and taking the powder average as defined in equation (25), the lth-order powder TDS is found from

$$I_{\mathrm{PTDS}_l}(s) = k(s)|f(s)|^2 \exp(-2M) A(s)^l \times \sum_{hkl} m_{hkl} \sum_{m,n} \frac{1}{2} \int_{\theta_{\min}}^{\theta_{\max}} \mathrm{sinc}(2\pi q_{hkl} d_{mn}) \times \frac{\left[(Y_{mn})_{\rm V} + (Y_{mn})_{\rm S} + (Y_{mn})_{\rm E}\right]^l}{l!} \sin\theta\,\mathrm{d}\theta, \quad (39)$$

where $q_{hkl}^2 = s^2 + s_{hkl}^2 - 2 s s_{hkl}\cos\theta$. Then, the powder TDS intensity becomes

$$I_{\mathrm{PTDS}_l}(s) = k(s)|f(s)|^2 \exp(-2M) A(s)^l \times \sum_{hkl} \frac{m_{hkl}}{2 s s_{hkl}} \sum_{m,n} \frac{\cos(2\pi d_{mn} g_0) - \cos(2\pi d_{mn} g_{\max})}{(2\pi d_{mn})^2} \times \frac{\left[(Y_{mn})_{\rm V} + (Y_{mn})_{\rm S} + (Y_{mn})_{\rm E}\right]^l}{l!}, \quad (40)$$

where

$$g_0 = \begin{cases} s - s_{hkl} & (s - s_{hkl}) \geq g_{\min} \\ g_{\min} & (s - s_{hkl}) < g_{\min} \end{cases}. \quad (41)$$

The double summation over m and n can be expressed as a single summation over the unique distances in the crystallite, d_i, and their multiplicity, m_i. For instance, if $d_0 = 0$, then $m_0 = N$, and one finds that the respective Y_0 functions are equivalent to those found in the D–W exponent of equation (18*b*). Then, the lth-order powder TDS for a given hkl reflection is

$$I_{\mathrm{PTDS}_l}(s, s_{hkl}) = \frac{k(s)|f(s)|^2 m_{hkl} \exp(-2M) A(s)^l}{2 s s_{hkl} l!} \times \left\{ N \frac{g_{\max}^2 - g_0^2}{2} \left[(Y_0)_{\rm V} + (Y_0)_{\rm S} + (Y_0)_{\rm E}\right]^l + \sum_{i>0} m_i \frac{\cos(2\pi d_i g_0) - \cos(2\pi d_i g_{\max})}{(2\pi d_i)^2} \times \left[(Y_i)_{\rm V} + (Y_i)_{\rm S} + (Y_i)_{\rm E}\right]^l \right\}. \quad (42)$$

Finally, using equation (6), the normalized TDS is given by

$$Q_l(s, s_{hkl}) = \frac{m_{hkl}}{2 s s_{hkl}} \left\{ \frac{g_{\max}^2 - g_0^2}{2} + \sum_{i>0} \frac{C_i}{(2\pi d_i)^2} \left[\cos(2\pi d_i g_0) - \cos(2\pi d_i g_{\max})\right] \times \frac{\left[(Y_i)_{\rm V} + (Y_i)_{\rm S} + (Y_i)_{\rm E}\right]^l}{\left[(Y_0)_{\rm V} + (Y_0)_{\rm S} + (Y_0)_{\rm E}\right]^l} \right\}, \quad (43)$$

where $C_i = m_i/N$.

A full evaluation of the sum is neither practical for large crystallites, nor generally necessary, as only the first few sets of nearest neighbors significantly contribute to this sum, owing to the $1/d_i^2$ dependence. Then, as suggested by Warren, we chose to explicitly evaluate the sum over the first eight nearest neighbors and found that it was enough for convergence of the sum. For a face-centered cubic (f.c.c.) crystal, the distance to the first eight nearest neighbors is given by $d_i = a(i/2)^{1/2}$ and the normalized multiplicities are $C_i = \{12, 6, 24, 12, 24, 8, 48, 6\}$.

Also, to approximate the convolution with the Bragg peak, we incorporated the size effect into the sum by weighting the multiplicities from a perfect lattice by the common volume function of the crystallite, $v(\mathbf{d}_i)$. The function $v(\mathbf{r})$ is sometimes described as the volume common to the particle and its 'ghost', and is responsible for size broadening of the Bragg peak (Beyerlein, Snyder & Scardi, 2011). The multiplicities were then given by $C_i = m_i v(\mathbf{d}_i)/N$. Owing to this strong dependence on only the first few nearest neighbors, adjusting the multiplicities by the finite crystallite size was only found to result in a slight change of the TDS, unless the crystallite size decreased to the range of the eight nearest neighbors used in evaluating the sum.

The resulting forms of a few higher-order TDS terms found from equation (43) are shown in Fig. 2(*d*). Again, the intensity scale of each order of the TDS in this figure is shown as that directly given from the expression for Q_l. In this figure, the higher-order peaks are found to be dramatically broader than the first-order TDS peaks. However, they influence the diffracted pattern much less, as equation (5) shows they must be scaled by $2M^l/l!$ to be in electron units.

The full TDS in principle includes an infinite number of higher-order terms. Simply neglecting to include some of them does not conserve the integrated intensity of the peak. Instead, we propose using an expression of the form

$$I_{\rm P} = \exp(-2M) I_{\rm Bragg} + I_{\rm PTDS_1} + I_{\rm PTDS_2} + \ldots + I_{\rm PTDS_{lmax}} + I_{\rm R}, \quad (44)$$

where *l*max represents the maximum TDS order which was evaluated using equation (43) and $I_{\rm R}$ represents the remaining intensity from the neglected higher-order terms,

$$I_{\rm R}(s) = \sum_{l=l{\rm max}+1}^{\infty} I_{{\rm PTDS}_l}(s). \quad (45)$$

An approximate analytical solution to this series can be found, given by

$$I_{\rm R}(s) = k(s) N |f(s)|^2 \sum_{hkl} Q_{l{\rm max}}(s, s_{hkl}) \left[1 - \frac{\Gamma(l{\rm max}+1, 2M)}{\Gamma(l{\rm max}+1)}\right], \quad (46)$$

where the functions $\Gamma(a, x)$ and $\Gamma(a)$ are, respectively, the incomplete gamma function and the gamma function. This form of the remaining intensity is found assuming that Q_l is equivalent to $Q_{l{\rm max}}$ for all $l > l{\rm max}$, which is shown to be a good approximation considering the similarity in shape of the third- and fourth-order peaks in Fig. 2(*d*).

2.3.5. TDS crystallite size dependence. Summing the expressions for the different orders of the TDS which have just been derived, we can study the effect that changing the largest allowed phonon wavelength, $\lambda_{\rm max}$, has on the total TDS. Fig. 3 contains plots of this type for three Al spheres whose sizes differ by orders of magnitude, and were simulated assuming an incident X-ray wavelength of $\lambda = 0.1$ nm. It is clear that a smaller $\lambda_{\rm max}$ results in a TDS function that is broader near the Bragg peaks and is observably more truncated. Also, it is interesting to note that this truncation effect is only expected to be observable in the TDS for crystallites that are smaller than 100 nm, as the TDS in this case does not dramatically differ from that of an infinite crystal. Finally, a crystallite with $\lambda_{\rm max} = 2$ nm shows the extreme case, as the TDS becomes effectively smoothed due to this truncation and broadening. However, at this extremely small size, the quantitative reliability of the proposed TDS is still questionable.

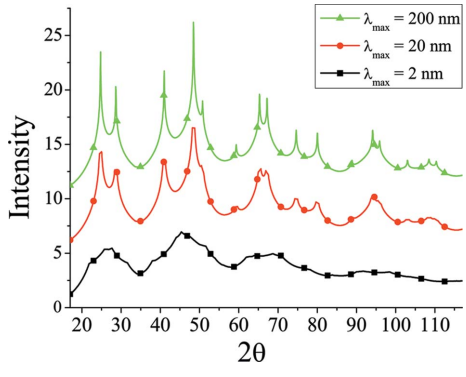

Figure 3
The total TDS intensities for Al spheres of different sizes are depicted; the parameters for Al are the same as those described in Fig. 1. These patterns are the result of summing the contributions from the first three TDS orders, including the remaining intensity, and assuming an incident radiation with $\lambda = 0.1$ nm. The patterns have been offset in the figure to allow for their clear distinction, and have been scaled by the number of atoms in each crystallite to allow for their direct comparison.

Specifically, at this size one should consider if the small crystallites have the same structure, and elastic behavior, as compared to thier bulk form.

The patterns shown in Fig. 3 only extend to an $s_{\rm max}$ of about 6.38 nm^{-1}, which is common for X-ray line profile analysis measurements in a laboratory setting, but is small compared to the full possible range of neutron and high-energy X-ray diffraction studies. In the limit of high s (or q, as it is commonly called in these scientific circles), the scale of the powder TDS becomes largely dictated by its power-law dependence on s, as well as the D–W factor. Therefore, ignoring for the moment the influence of the atomic scattering factor and other instrumental factors, the *l*th-order TDS for large values of s can be approximated as being proportional to

$$I_{{\rm PTDS}_l} \propto s^{2l} \exp(-2M) = s^{2l} \exp\left(-B_{\rm iso} s^2/2\right). \quad (47)$$

This function rises to a maximum at some relatively large value of s and is then driven to zero by the D–W factor (Warren, 1990; Willis & Pryor, 1975). The scattering vector magnitude for which this function takes a maximum, $s_{\rm max}$, is found from differentiation of equation (47) to be

$$s_{\rm max} = \left(\frac{2l}{B_{\rm iso}}\right)^{1/2}. \quad (48)$$

As it has already been shown in §2.3.2 that $B_{\rm iso}$ is size dependent, then our model also predicts that this turnover point for the TDS should be size dependent. The trend of $s_{\rm max}$ for the first-order TDS of Al crystallites is then given in Fig. 4 as a function of crystal size. It is seen that as the crystal size decreases the location of this maximum shifts to lower scattering vectors. For the case considered here, this shift becomes significant and more observable for crystal sizes below 200 nm. The corresponding turnover points for higher-order TDS contributions are expected to follow the same general trend, as found from equation (48), that the positions of the relative peaks are found by scaling that of the first-order by a factor of $l^{1/2}$.

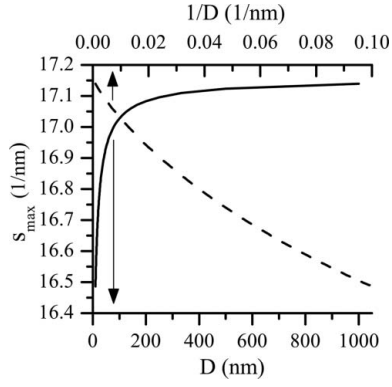

Figure 4
The scattering vector magnitude where the first-order TDS reaches a maximum in the high s approximation $s_{\rm max}$ is shown as a function of crystal size for the case of Al spheres. The physical constants used to calculate this relation follow those given previously in Fig. 1, with $c_{\rm l}/c_{\rm t} = 1$.

2.3.6. Approximations and practical implementation. It is important to review the series of rather limiting approximations which were necessary to arrive at the expressions for the TDS which have just been presented. As already pointed out in the text, a simple linear dispersion relationship and a high-temperature approximation to the energy distribution function were used. Also, the influence of optical vibration modes was not included, as only the influence of the acoustic branch was described. The density of states is then treated in terms of the long-wavelength approximation which, for the volume component, follows a quadratic dependence on the wavevector, often called the Debye density of states. In order to carry out many of the integrals, it was necessary to approximate the shape of the Brillouin zone as a sphere of equal volume. Also, since the speed of sound was not given in terms of the elastic constants, and thereby not allowed to be directionally dependent, the form of the TDS devised here is only appropriate for nearly elastically isotropic materials. Finally, the elastic properties of the surface, in terms of the speed of sound, are assumed to be the same as those of the bulk, which is not generally true.

More subtly, atomic vibrations were approximated as harmonic oscillations and the effects of anharmonicity have not been included. This approximation begins to break down for temperatures that are high relative to the Debye temperature. Also, recent inelastic neutron and γ-ray scattering experiments have observed an increase in the low-energy regime of the phonon density of states of nanocrystalline metals, and have attributed it to a decreased lifetime of phonons in a *damped* harmonic oscillator model (Fultz *et al.*, 1997; Roldan Cuenya *et al.*, 2009).

Finally, isolated crystallites are assumed. This makes this model more appropriate to describe the diffraction pattern from nanoparticles grown by chemical syntheses, instead of that of dense nanocrystalline materials which have been formed by severe deformation. This latter microstructure can exhibit coupled vibrations between grains and contain amorphous regions which are believed to lead to different vibrational characteristics (Suck, 2007), and invariably different forms of the D–W factor and TDS.

These approximations were made to keep the number of free parameters, and level of complexity, of the model to a reasonable level. Many are commonly found in the more widely used powder diffraction TDS models (Suortti, 1967; Warren, 1990). Concerning the linear dispersion approximation, slight changes in the shape of the first-order TDS have been found when considering that of a linear chain of oscillators (Suortti, 1967). However, Walker & Chipman (1972) have found that the error in using a linear dispersion relationship can somehow be offset by also assuming the same velocity of sound for longitudinal and transverse modes, or $c_l/c_t = 1$. In any case, if one does not require an analytical solution for the powder TDS, expressions for the TDS in terms of the elastic constants of the material, and correct dispersion relationship, can be introduced into the model and evaluated numerically (Walker & Chipman, 1972). This last consideration is necessary to correctly describe the TDS from elastically anisotropic cubic materials.

Use of our TDS in a pattern modeling procedure adds only three additional physical parameters to the refinement: the longitudinal and transverse speed of sound, c_l and c_t; and the maximum phonon wavelength, λ_{max}. The other parameters are either best assumed to be known, like the temperature and atomic mass, or are coupled to the values governing Bragg scattering, such as the crystallite size, L, and lattice parameter, a. However, because of the large number of approximations which have gone into formulating the TDS, the obtained speeds of sound and λ_{max} are better considered relative, instead of absolute, measures of the vibrational properties of a material.

It is important to point out that the dimensionality of the effect of surface and edge modes is embodied in the presented expressions. However, in practice it may be useful to relax some of the rigidity of the model. For instance, some further parameters can be implemented to change the scale factors of the surface and edge modes. This tweaking allows for more flexibility to model the shape of the VDOS, and can be used to account for cases when the approximations made in developing the model begin to break down.

Again, it should be kept in mind that the TDS relations and plots which have been depicted here are somewhat idealized as they have not been convolved with the existing Bragg peak shape. As long as the Bragg peak is relatively sharp, and symmetrical, compared to the TDS, this convolution will only effectively round off the top of the TDS and smooth any sharp corners which are present in Fig. 3. In practice, this effect is hardly observable as the truncated portion of the TDS is under the Bragg peak. A rough calculation finds that broadening of the TDS in the tails as a result of this convolution will only be observable when the size decreases to about 1 nm, which approaches the limit of what can even be considered a crystallite.

Also, in the modeling of an experimental pattern, it is important to consider that other phenomena are known to contribute to the background, including Compton scattering, air scattering and background radiation. In a complete *ab initio* approach, models for each one of these phenomena must also be assumed and refined.

3. Simulated patterns

The described expressions for the TDS have been implemented into the line profile analysis software *PM2K* (Leoni *et al.*, 2006), which is based on the whole powder pattern modeling (WPPM) approach to powder diffraction pattern analysis (Scardi & Leoni, 2002). This analysis tool already contains accurate expressions for the generation of the component of the powder Bragg peaks due to the size and shape of spherical crystallites (Scardi & Leoni, 2001). So, it allows for generation of the full diffraction pattern, including the TDS and Bragg component.

A series of diffraction patterns were then simulated for Al spheres of different sizes and temperatures. As is the

conventional understanding, the TDS was found to add to the observed background and influence the peak shape by slightly broadening the diffraction peak tails. When a smooth function is used to approximate the TDS, it is then possible that this apparent broadening can be misunderstood as size broadening, or some other kind of strain broadening. In an attempt to quantify the resulting error, simulated patterns of Al spheres of different sizes, and including the TDS at different temperatures, were then treated as experimental data and modeled assuming different representations of the thermal background. In all cases, patterns were simulated assuming an incident radiation wavelength $\lambda = 0.1$ nm over the 2θ range of 17 to 117°.

Three models were considered to represent the thermal background in the modeling. First, a sixth-order Chebyshev background was assumed following the arguments of §2.1. Next, the Debye background, given by equation (4), was used. Finally, the patterns were modeled only considering the volume contribution to the TDS, which is obtained from the previous relationships by setting the S/V and E/V ratios equal to zero. This final model is then a test of the necessity to include the surface and edge contributions when modeling the powder diffraction TDS from small crystallites. The goal of the modeling was then to compare the obtained best-fit parameters with those used in the diffraction pattern generation. In the cases of the Debye background and volumetric TDS, the same value for the B_{iso} parameter was used to determine the D–W factor and background function.

An example of the quality of fit which is obtained in the modeling is depicted in Fig. 5(*a*) for the case of a 5 nm Al sphere at 300 K. Also, the Chebyshev polynomial and Debye background which resulted in the best fit of this pattern are compared to the full TDS in Fig. 5(*b*). Though the quality of the fit is quite good, it is clearly apparent that the Chebyshev and Debye background are not able to mimic the shape of the TDS.

Patterns from the 5 nm sphere were simulated for a series of temperatures between 300 and 900 K. As the temperature was increased, the peaks of the TDS, like those shown in Fig. 5(*b*), became more apparent. Thus, the ability of the other models to fit the data became worse. At the same time, the best-fit parameters for the crystallite size and D–W parameter were found to deviate more from the expected values. Fig. 6 shows that, as the simulated temperature was increased, both the obtained parameters were found to be increasingly underestimated. In essence, the fitting routine attempted to compensate for the missing TDS peaks by raising the Bragg peak height (decreasing B_{iso}) and by increasing the peak breadth (decreasing D). Notably, the error in the crystallite size was only found to be on the order of a few percent when using the Chebyshev and Debye backgrounds, even for this small crystallite size. This same degree of error was also found in a similar study where the diffraction patterns were simulated from molecular-dynamics simulations of Al nanoparticles (Beyerlein, Leoni *et al.*, 2011). However, the difference in the obtained B_{iso} is more striking, as an error in the range of 20–40% was found when assuming these smooth background functions. It is believed that these deviations are a result of the inability of the respective assumed models to represent the features in the data, and while they give some

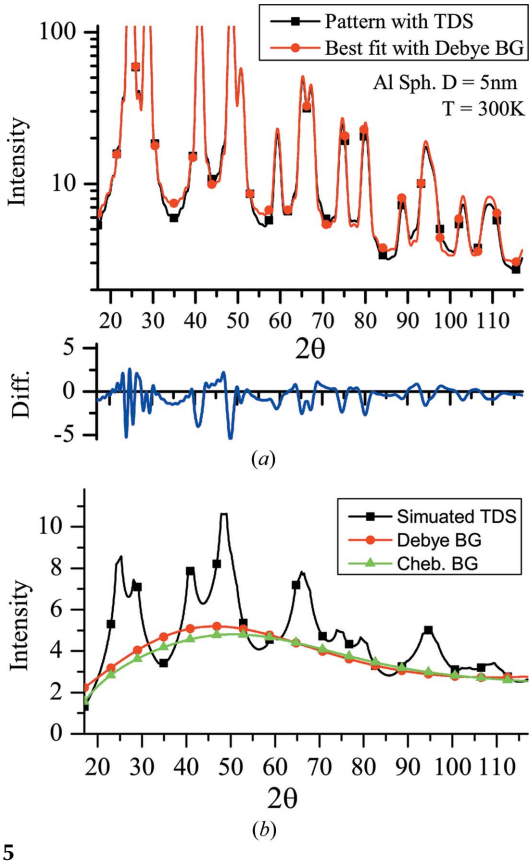

Figure 5
(*a*) An example of the quality of fit obtained in modeling the simulated pattern from a 5 nm Al sphere at 300 K is shown, with the difference between the fit and the simulated pattern depicted below. (*b*) The Debye and Chebyshev background functions which resulted in the best fit of the simulated pattern are compared to the total TDS which was used.

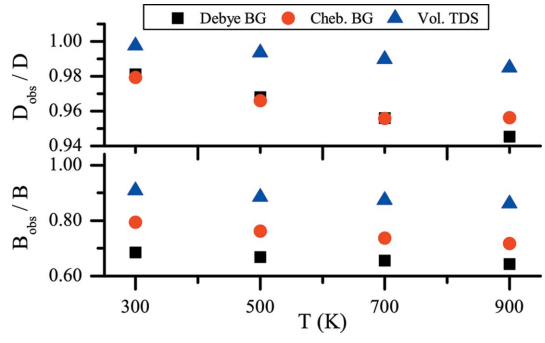

Figure 6
Depicted are trends of how the observed crystallite size and D–W parameter, scaled by the expected value, change with the simulated temperature. These values were obtained from modeling the patterns from $D = 5$ nm Al spheres, assuming $c_l = c_t = 6420$ m s^{-1}. In the plots, squares correspond to assuming the Debye background function (Debye BG) defined in equation (4), circles denote a Chebyshev background (Cheb. BG) as defined in equation (3), and triangles are the results assuming only the volumetric contribution to the TDS (Vol. TDS).

insight into the expected magnitudes and trends, they will be different for other materials on a case-by-case basis.

From Fig. 6 it is apparent that the Chebyshev background is slightly better at obtaining the correct D–W parameter than the Debye background. This result is possibly due to the increased flexibility of the Chebyshev model. Still, as shown in Fig. 5(*b*), the best-fit Chebyshev background does not differ terribly in its form from that of the Debye background. This is evidence that the Bragg peak height, as determined by the D–W parameter, is highly sensitive and correlated to the background in powder diffraction pattern analysis.

Patterns were also simulated for a series of diameters ranging from 3 to 100 nm. A study of the temperature dependence of the fit for each size found similar trends to those just described for the case of a 5 nm sphere. An analysis of how the error in the obtained diameter and B_{iso} change with size, for a temperature of 300 K, is shown in Fig. 7. It is found from these figures that the obtained parameters are again underestimated in all cases, while an increasing magnitude of error was found with decreasing size. This trend is explained as a result of the TDS peaks becoming more apparent relative to the Bragg peaks as the size decreases, thereby requiring more adjustment of the D and B_{iso} parameters to account for its presence. This affirms the primary motivation for this study, which was the assertion that it becomes more important to properly consider the TDS with smaller crystals. Conversely, these trends also show that it is indeed a relatively good approximation to ignore the TDS when modeling the diffraction pattern from large crystallites, at room temperature. In this light, Fig. 7 shows that the error of the D–W parameter goes below 10% for crystallites larger than 100 nm, when using a Chebyshev background in our simulations.

Also shown in Figs. 6 and 7 are the results of modeling the simulated patterns assuming a TDS which only consists of the volumetric phonon modes. It is clear that this form of the TDS dramatically improves the accuracy of the obtained physical parameters. In this case a more accurate determination ofthe crystallite size is understood considering that it includes the primary contribution to the broadening in the peak tails. Also,

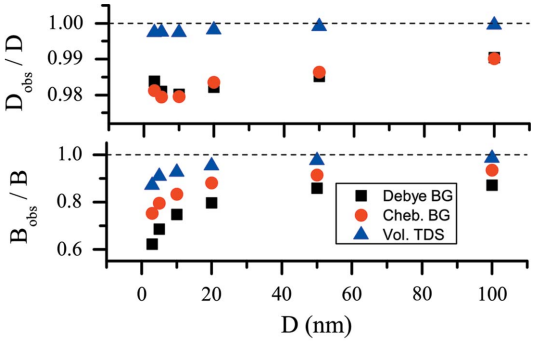

Figure 7
The depicted trends show how the observed crystallite size and D–W parameter, scaled by the expected value, change with the assumed crystallite size. The case of Al spheres at a temperature of 300 K and $c_l = c_t = 6420$ m s^{-1} were assumed in simulating the patterns. The symbols used in these plots correspond to the same backgrounds that are described in the caption of Fig. 6.

in our simulations it was found that in this case the obtained value of B_{iso} begins to deviate for crystallite sizes below 50 nm. This gives an estimate of the size range when it becomes necessary to consider the influence of surface and edge modes.

Simulations were also carried out assuming a smaller incident radiation wavelength, extending the maximum observed s from about 10 nm^{-1} in the present case, up to 15 nm^{-1} – which more than doubles the number of observed peaks. The percent errors of B_{iso} and D which were found for these cases differed by less than 1% from those that have already been presented. This suggests that the results of this study are largely independent of the range of reciprocal space which has been simulated, or might be measured. This observation again hints that the fundamental flaw in using a smooth function to represent the TDS is not an inability to mimic the general trend of the TDS, but is instead the neglect of the fine details which the TDS contributes near the Bragg peaks.

4. Conclusion

A complete model for the powder TDS of small crystallites has been described, which demonstrates the general effects of surface and edge vibration modes, as well as a maximum phonon wavelength. It has also been shown that assuming a smooth Chebyshev polynomial, or Debye background function, is a poor approximation to the TDS. This inaccuracy in the modeling is found to lead to an underestimation of the obtained D–W parameter, as well as crystallite size – which in more general terms represents an inaccurate determination of the line profile broadening. This error was shown to increase as the crystallite size decreased, when assuming these smooth background functions. Therefore, it was found that consideration of the TDS was important when modeling the diffraction pattern from nanocrystalline materials. Specifically, this study has shown that this is most important for scientists to consider when either reporting, or using, data on the Debye–Waller factor in diffraction studies.

While this study has focused on the development of the TDS theory for X-ray powder diffraction measurements, the methodology, and some of the resulting relations, can also be useful to describe similar effects in other measurements. For example, in order to arrive at the powder intensity, one must first describe that from the single crystal. So, someone interested in testing the theory for this kind of measurement need only use the relations found before taking the powder average [*i.e.* equations (24) and (37)]. Furthermore, neutron diffraction measurements can also contain similar TDS effects. As it turns out, if the speed of the neutrons is faster than the speed of sound in the material, then the temperature diffuse scattering observed in neutron diffraction follows the same form as in X-ray diffraction (Willis & Pawley, 1970; Willis & Pryor, 1975). So, we also expect our relations to be useful in describing the TDS for this kind of neutron powder diffraction measurement.

This work would not have been possible without the help and support of the late Dr Robert L. Snyder, to whom this manuscript is dedicated.

References

Balerna, A. & Mobilio, S. (1986). *Phys. Rev. B*, **34**, 2293–2298.
Beyerlein, K. R., Leoni, M., Snyder, R. L., Li, M. & Scardi, P. (2011). *Z. Kristallogr. Proc.* **1**, 43–48.
Beyerlein, K. R., Snyder, R. L. & Scardi, P. (2011). *J. Appl. Cryst.* **44**, 945–953.
Bolt, R. (1939). *J. Acoust. Soc. Am.* **10**, 228–234.
Born, M. & Huang, K. (1998). *Dynamical Theory of Crystal Lattices.* Oxford University Press.
Couchman, P. & Karasz, F. (1977). *Phys. Lett. A*, **62**, 59–61.
Debye, P. (1914). *Ann. Phys.* **43**, 49–94.
Eastman, J. & Fitzsimmons, M. (1995). *J. Appl. Phys.* **77**, 522–528.
Fultz, B., Ahn, C., Alp, E., Sturham, W. & Toellner, T. (1997). *Phys. Rev. Lett.* **79**, 937–940.
Honkimäki, V. & Suortti, P. (1992). *J. Appl. Cryst.* **25**, 97–104.
Inagaki, M., Sasaki, Y. & Sakai, M. (1983). *J. Mater. Sci.* **18**, 1803–1809.
James, R. W. (1962). *The Crystalline State*, Vol. II, *The Optical Principles of the Diffraction of X-rays*, pp. 193–210. London: G. Bell and Sons.
Leoni, M., Confente, T. & Scardi, P. (2006). *Z. Kristallogr.* **23** (Suppl.), 249–254.
Maa, D. (1939). *J. Acoust. Soc. Am.* **10**, 235–238.
Marshall, S. & Wilenzick, R. (1966). *Phys. Rev. Lett.* **16**, 219–221.
Montroll, E. W. (1950). *J. Chem. Phys.* **18**, 183–185.
Press, W. H., Teukolsky, S. A., Vetterling, W. T. & Flannery, B. P. (2007). *Numerical Recipes: the Art of Scientific Computing*, 3rd ed., pp. 233–238. New York: Cambridge University Press.
Roe, G. (1941). *J. Acoust. Soc. Am.* **13**, 1–7.
Roldan Cuenya, B., Croy, J., Ono, L., Naitabdi, A., Heinrich, H., Keune, W., Zhao, J., Sturhahn, W., Alp, E. & Hu, M. (2009). *Phys. Rev. B*, **80**, 1–7.
Sadaiyandi, K. (2009). *Mater. Chem. Phys.* **115**, 703–706.
Scardi, P. & Leoni, M. (2001). *Acta Cryst.* A**57**, 604–613.
Scardi, P. & Leoni, M. (2002). *Acta Cryst.* A**58**, 190–200.
Schoening, F. R. L. (1968). *Acta Cryst.* A**24**, 615–619.
Solliard, C. (1984). *Solid State Commun.* **51**, 947–949.
Suck, J. (2007). *Materials for Tomorrow*, ch. 6, pp. 147–190. New York: Springer.
Suortti, P. (1967). *Ann. Acad. Sci. Fenn.* **240**, 7–32.
Suortti, P. (1993). *The Rietveld Method*, ch. 9. International Union of Crystallography Monographs on Crystallography 5. Oxford University Press.
Thiel, R. (1967). *Z. Phys. A*, **200**, 227–238.
Urban, J. P. (1975). *Acta Cryst.* A**31**, 95–100.
Walker, C. B. & Chipman, D. R. (1972). *Acta Cryst.* A**28**, 572–580.
Warren, B. E. (1990). *X-ray Diffraction*, pp. 151–201. Reading: Dover.
Willis, B. T. M. & Pawley, G. S. (1970). *Acta Cryst.* A**26**, 254–259.
Willis, B. T. M. & Pryor, A. (1975). *Thermal Vibrations in Crystallography.* London: Cambridge University Press.
Xiong, S., Qi, W., Cheng, Y., Huang, B., Wang, M. & Li, Y. (2011). *Phys. Chem. Chem. Phys.* **13**, 10652–10660.
Zhao, Y. & Lu, K. (1997). *Phys. Rev. B*, **56**, 14330–14337.